Supporting Information

Castaing et al. 10.1073/pnas.1210554110

SI Materials and Methods

General Methods. To determine sporulation efficiencies, cells were grown and induced to sporulate in Difco Sporulation Medium (KD Medical) for at least 24 h; nonsporulating cells were killed by exposure to 80 °C for 20 min. Mutations in SpoIVA (hereafter called IVA) were introduced using the QuikChange Lightning Site-Directed Mutagenesis kit (Agilent) and utilizing plasmid pKR145, pKR13, or pKR130 as a template (1). Mutagenesis was confirmed by DNA sequencing. IVA levels in sporulating cells were determined by immunoblotting cell extracts prepared as described previously (1) using rabbit antiserum raised against purified IVA (Covance, Inc.).

His_6-IVA Purification. To purify His_6-IVA from *Escherichia coli* BL21(DE3) pKR145 and derivatives, cultures grown at 37 °C in LB containing 50 mg/mL kanamycin were grown to mid-logarithmic phase. Isopropyl-β-D-thiogalactopyranoside was added to 1 mM final concentration, and the culture was grown for 4 h at 37 °C. Harvested cells were resuspended in 35 mL of ice-cold buffer A [50 mM Tris (pH 7.5), 150 mM NaCl] and disrupted by French press. All subsequent steps were performed at 4 °C; proteins were monitored by SDS/PAGE, and protein concentrations were estimated by the Bradford assay (BioRad) and by A_{280} Nanodrop spectrophotometer measurements (ND-1000, Thermo Scientific). Unbroken cells and cell debris were removed by centrifugation at 30,000 × *g*, and the cleared lysate was loaded on Histrap FF columns (1 mL; GE Healthcare) and washed successively with 5 mL of buffer A containing 20 mM, 40 mM, or 80 mM imidazole. Bound protein was eluted with buffer A containing 200 mM imidazole. Peak fractions were identified and pooled. Imidazole was removed by applying the sample onto a PD-10 desalting column (1 mL; GE Healthcare) and eluted using buffer A. Peak fractions were identified, pooled, and separated by ion exchange chromatography (mono-Q; Pharmacia) and then eluted with a linear gradient of 150–1,000 mM NaCl; His_6-IVA routinely eluted at 0.4 M NaCl. Purified His_6-IVA was stored at 4 °C and was used in less than 48 h after purification due to precipitation of the protein on prolonged storage. For total internal reflection fluorescence (TIRF) experiments, purified proteins were labeled with Alexa Fluor 647 C2-maleimide or Alexa Fluor 488 C5-maleimide (Life Technologies) as described by the manufacturer.

ATP Binding and Hydrolysis Assays. Different concentrations of purified His_6-IVA were incubated for 1 min in 10 μL of buffer A containing 10 mM $MgCl_2$ with 7 nM [α-^{32}P]-ATP. The entire sample was spotted onto a dry nitrocellulose membrane, allowed to dry, exposed to a phosphor screen (Storm 860 phosphoimager; GE Healthcare) for imaging, and analyzed with Fujifilm MultiGauge software. Release of ADP and phosphate over time was also analyzed using the differential radial capillary action of ligand assay (DRaCALA) technique in the same buffer conditions with 5 μM purified His_6-IVA and with 7 nM [α-^{32}P]-ATP or [γ-^{32}P]-ATP, respectively. ATPase activity was measured by monitoring ADP formation during incubation of 2 μM purified His_6-IVA in 10 μL of buffer A containing 10 mM $MgCl_2$, 1 mM cold ATP, and 40 nM [α-^{32}P]-ATP. Reactions were incubated at 37 °C for 4 h and quenched by addition of 10 μL of 3 mM ATP, 3 mM ADP, and 50 mM EDTA. A total of 2.5 μL of each sample was applied to a TLC plate, and the chromatograph was developed with 1 M formic acid/LiCl. The plates were dried, exposed to a phosphor screen, and analyzed.

In Vitro Polymerization Assays. ***Centrifugation.*** The specified concentration of purified His_6-IVA was incubated in a 100-μL reaction volume in buffer C [50 mM Tris·HCl (pH 7.6), 400 mM NaCl, 10 mM $MgCl_2$] in the presence or absence of 4 mM ATP at 37 °C for the specified period. Where indicated, 1 unit of apyrase from potato (Sigma) was added. Samples were centrifuged at 100,000 × *g* for 30 min at 4 °C. The supernatant (95 μL) was removed from each tube, and the pellet was resuspended in an equal volume of buffer C. Samples were separated by PAGE and analyzed by Coomassie staining. Visualized bands were quantified, and the percentage of protein present in the pellet was calculated. Nonlinear regression analyses to fit data to the Hill model were performed using Prism 5 software (GraphPad Software, Inc.). To measure nucleotide association with polymerized IVA, 160 nM [α-^{32}P]-ATP was added to the polymerization assay and radioactivity associated with the pellet fraction at different time points was evaluated by Cerenkov counting. Before centrifugation, at each time point, ATP hydrolysis was measured by TLC as described above. To test the stability of IVA polymers, purified IVA was allowed to polymerize for 16 h as described above. The reaction mix was then diluted threefold with buffer C containing 4 mM ATP and incubated at 37 °C. At different time points, samples were centrifuged and the amount of IVA in the supernatant and pellet fractions was determined by gel electrophoresis and Coomassie staining as described above.

TIRF microscopy. TIRF experiments were performed at 25 °C in buffer C containing 4 mM ATP. The final concentration of fluorescently labeled proteins in the assay mixture was 3 μM; in case of mixing experiments, the molar ratio of individual proteins was 1:1. The TIRF assay was performed on an Olympus IX70 microscope equipped for objective type TIRF using a PlanAPO (100×, 1.49 n.a.) objective lens, an Olympus motorized multicolor cell TIRF illuminator, and a relay lens (PE5, 5× PE2.5, 2.5×; Olympus) connected to an electron multiplying CCD (Andor Technology) and a two-color observation system (dual view system; Optical Insights). The excitation light sources were 488- and 647-nm diode lasers (IK Series He-Cd laser, Kimmon Koha Co.). To prevent nonspecific binding of fluorescently labeled protein, the coverslips (upper, 18 × 18 mm; lower, 24 × 50 mm) comprising the flow cell were prepared by soaking in concentrated H_2SO_4 overnight, washed extensively with warm water, and dried with a stream of nitrogen. The flow cell, ∼30 μL in volume, was prepared using double-sided Scotch tape (3M). Data were captured and analyzed using the MetaMorph (Universal Imaging) software package.

EM. Three micromolar purified His_6-IVA was incubated in a 100-μL reaction volume in buffer C in the presence or absence of 4 mM ATP at 37 °C for 24 h. Specimens were prepared for EM using the conventional negative staining procedure: Samples were adsorbed to freshly glow-discharged, carbon-coated grids; rinsed with water; and stained with 1% uranyl acetate. To avoid unspecific aggregation, the polymerized material was not centrifuged. Images were recorded on a Hitachi H7650 microscope with an Advanced Microscopy Techniques CCD camera.

Dynamic light scattering. Purified IVA in buffer C (100-μL reaction volume) was incubated in the presence or absence of 4 mM ATP for the specified period. Pressure dialysis to increase concentration was performed using Centricon filters. Samples were exposed to laser light in a DynaPro NanoStar System photometer (Wyatt); scattered light was measured as photons per second and analyzed using Dynamics V6 software (Novell).

Epifluorescence Microscopy. Overnight cultures of *B. subtilis* were induced to sporulate by the resuspension method (2). Cells were harvested at the indicated times, resuspended in PBS containing 1 $\mu g \cdot mL^{-1}$ fluorescent dye FM4-64 to visualize membranes, and placed on a glass- bottomed culture dish (Mattek Corp.). A 1% agarose pad made with distilled water was cut to size and placed on top of the cell suspension. Cells were viewed with a DeltaVision Core microscope system (Applied Precision) equipped with an environmental control chamber. Images were captured with a Photometrics CoolSnap HQ2 camera. Seventeen planes were acquired every 0.2 μm at 22 °C, and the data were deconvolved using SoftWorx software (GE Healthcare). At the sporulation time points that we examined, phase bright forespores had not yet developed; thus, the autofluorescence of forespores was not higher than background fluorescence. Additionally, control experiments with sporulating strains that did not harbor a *gfp* fusion indicated that the level of GFP fluorescence from fusions to IVA was well above the limited background fluorescence of the cells.

Fluorescence Labeling of Purified IVA. Fluorescent reagent was slowly mixed with protein (10:1 ratio) and incubated for 2 h at room temperature. Free label was separated from labeled protein by applying the sample onto a PD-10 desalting column and elution with buffer B [50 mM Tris (pH 7.5), 400 mM NaCl]. Peak fractions were identified and concentrated by means of Amicon ultra columns with a 10-kDa cutoff (Millipore).

1. Ramamurthi KS, Losick R (2008) ATP-driven self-assembly of a morphogenetic protein in *Bacillus subtilis*. *Mol Cell* 31(3):406–414.

2. Sterlini JM, Mandelstam J (1969) Commitment to sporulation in *Bacillus subtilis* and its relationship to development of actinomycin resistance. *Biochem J* 113:29–37.

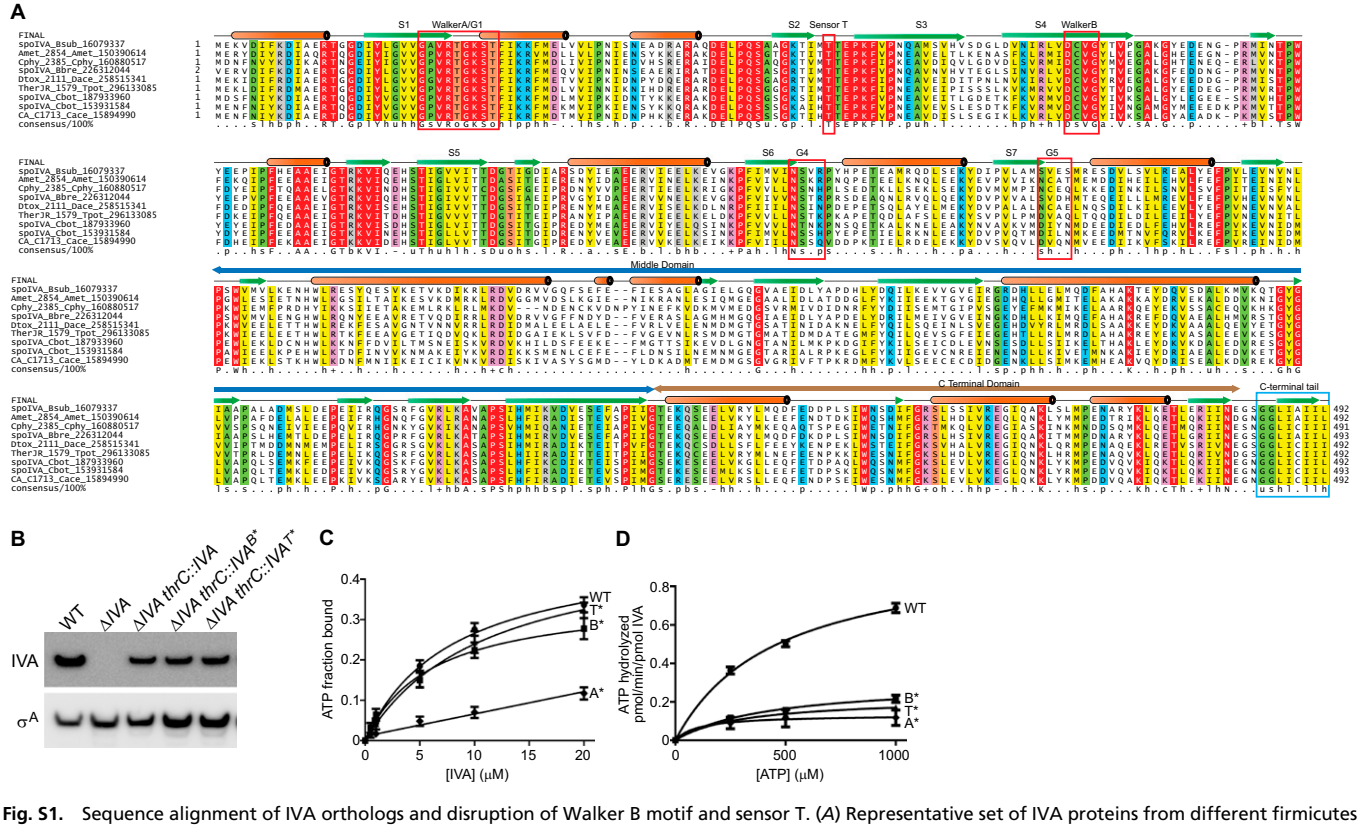

Fig. S1. Sequence alignment of IVA orthologs and disruption of Walker B motif and sensor T. (*A*) Representative set of IVA proteins from different firmicutes is shown in multiple sequence alignment. The active site residues of the GTPase domain are marked with red boxes. The middle domain is indicated with a blue marker, and the C-terminal domain is indicated with a brown marker. The conserved hydrophobic C-terminal tail is shown with a blue box. The secondary structure from the Era crystal structure is shown above the alignment with the orange cylinders representing helices and the green arrows representing β-strands, and the strands are numbered as in Fig. 1*B*. The 100% consensus shown below the alignment was derived for the IVA alone using the following amino acid classes: hydrophobic (h: ALICVMYFW, yellow shading), small (s: ACDGNPSTV, green), polar (p: CDEHKNQRST, blue) and its charged subset (c: DEHKR, pink), and big (b: FILMQRWYEK; gray shading). The species abbreviations are as follows: Amet, *Alkaliphilus metalliredigens*; Bbre, *Brevibacillus brevis*; Bsub, *Bacillus subtilis*; Cace, *Clostridium acetobutylicum*; Cbot, *Clostridium botulinum*; Cphy, *Clostridium phytofermentans*; Dace, *Desulfotomaculum acetoxidans*; and Tpot, *Thermincola potens*. (*B*) Disruption of the Walker B motif or sensor T does not affect the stability of IVA. Immunoblot analysis of cell extracts taken at 2.5 h after the induction of sporulation using antibodies to IVA. (*Upper*) Analyzed were extracts from WT cells (strain PY79) and cells producing no IVA (Δ*IVA*, strain KP73) or IVA^{WT} (strain KR394), IVA^{B*} (strain JPC221), or IVA^{T*} (strain JPC221) from an ectopic locus on the chromosome (*thr*). (*Lower*) Analysis of the same strain of cells using antibodies to σ^A, which is constitutively produced. (*C*) Saturation binding curve for IVA–ATP interaction. Varying concentrations of purified IVA (●), IVA^{A*} (♦), IVA^{B*} (■), or IVA^{T*} (▲) were incubated with a limiting amount of [α-^{32}P]-ATP, and the fraction of radiolabeled ATP bound to protein was determined using the differential radial capillary action of ligand assay. (*D*) Varying concentrations of radiolabeled [α-^{32}P]-ATP were incubated with purified IVA or IVA variants, and ADP production was measured using TLC. Symbols represent mean values of at least three independent measurements; error bars represent SEM.

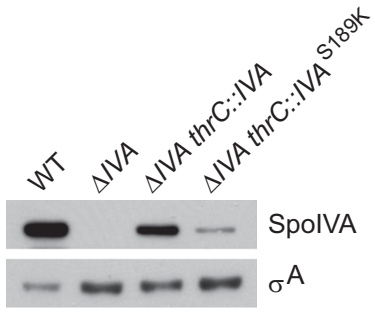

Fig. S2. Diminished accumulation of IVA^{S189K} in cell extracts of *Bacillus subtilis*. Immunoblot analysis of extracts from WT (strain PY79), Δ*IVA* (strain KP73), or Δ*IVA* complemented with either WT *IVA* (strain KR394) or *IVA*^{S189K} (strain JPC230) using antisera to detect SpoIVA (*Upper*) or σ^{A} (*Lower*).

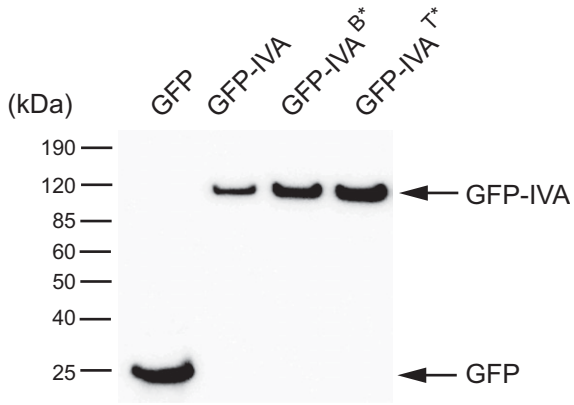

Fig. S3. In vivo stability of GFP fusions to IVA. Immunoblot analysis of extracts from cells producing GFP (strain MF339), GFP-IVA (JPC156), GFP-IVA^{B*} (JPC174), or GFP-IVA^{T*} (strain JPC243) prepared 2.5 h after the induction of sporulation. Strain genotypes are listed in Table S1.

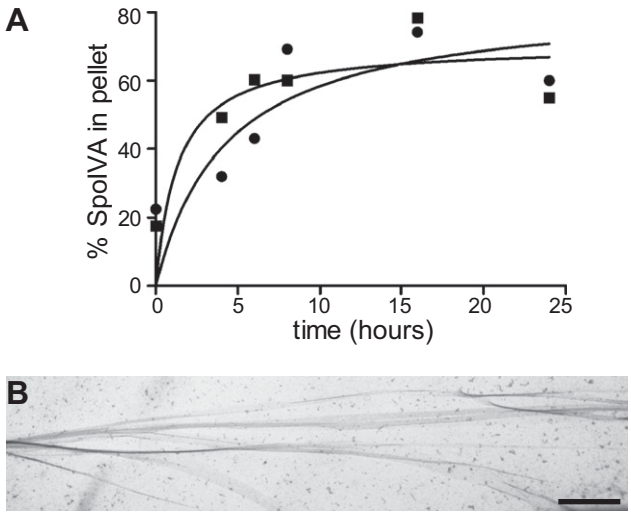

Fig. S4. ATP-dependent polymerization of IVA. (*A*) Addition of an ATP regeneration system does not significantly affect IVA polymerization. Kinetic analysis of polymerization of purified IVA either with (■) or without (●) the ATP regeneration system was performed and measured by centrifugation. Symbols represent a single representative measurement. (*B*) Purified IVA polymerizes into long, rigid filaments. A transmission electron micrograph of purified IVA at low magnification is visualized by negative staining. (Scale bar: 10 mM.)

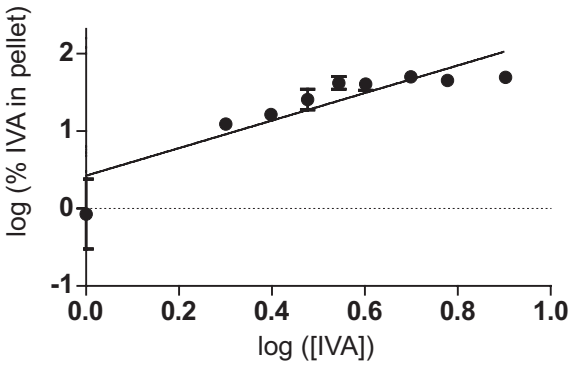

Fig. S5. Determination of the critical concentration for IVA polymerization. Data in Fig. 2*E* were plotted on a logarithmic scale. The *y*-intercept was 0.42 ± 0.14, the inverse log of which is ~2.7. Symbols represent mean values of at least three independent measurements; error bars represent SEM.

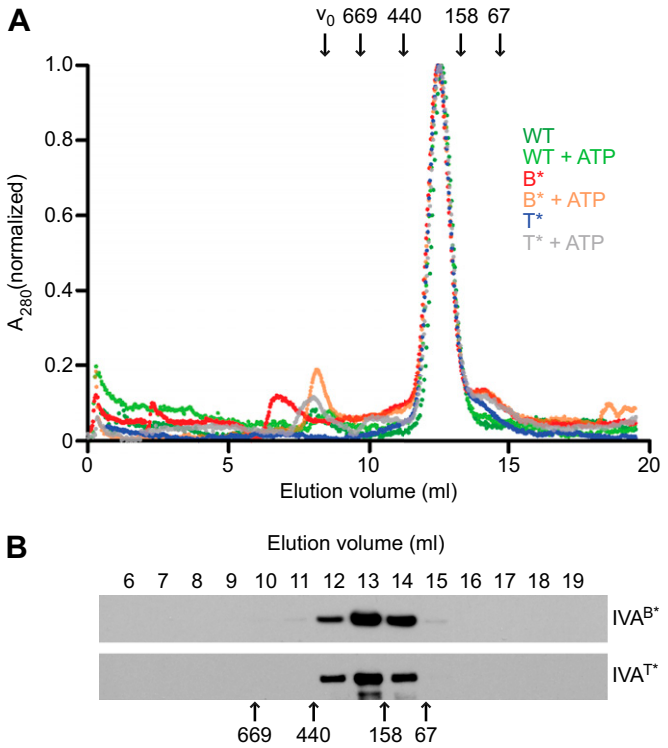

Fig. S6. ATP binding alone does not affect the oligomerization state of IVA or IVA variants. (*A*) Below-threshold concentration for polymerization. Two micromolar purified IVA (dark green and light green), IVA^{B*} (red and orange), or IVA^{T*} (blue and gray) was incubated without or with ATP, respectively, for 4 h at 37 °C and separated by size exclusion chromatography (Superdex 200; GE Healthcare). Absorbance was normalized for each sample relative to its highest and lowest values. (*B*) Above-threshold concentration for polymerization. Four micromolar purified IVA^{B*} or IVA^{T*} was incubated with ATP for 4 h at 37 °C and separated by size exclusion chromatography. One-milliliter fractions were examined by immunoblotting using antisera to detect IVA. The elution peaks for dextran (v0, void volume), thyroglobulin (669 kDa), ferritin (440 kDa), aldolase (158 kDa), and BSA (67 kDa) are indicated with arrows.

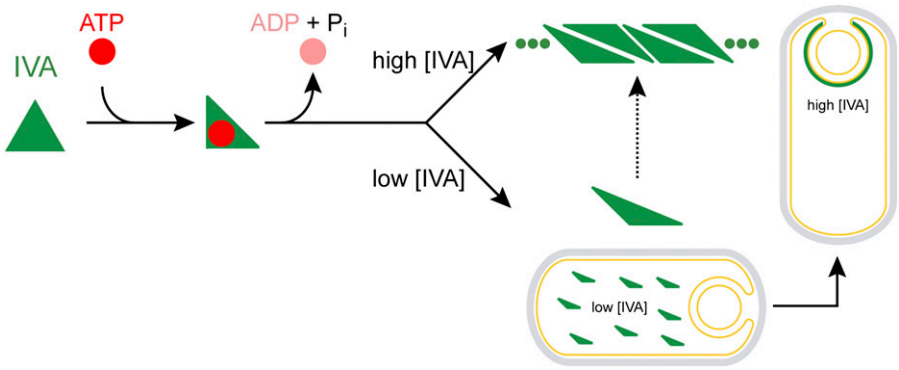

Fig. S7. Model for the role of ATP hydrolysis during assembly of the basement layer of the spore coat. Minimal assembling units of SpoIVA (perhaps trimers) produced in the mother cell of *Bacillus subtilis* during sporulation (green equilateral triangle) bind ATP (red), which results in a conformational change (right triangle). The bound ATP is then hydrolyzed, and the resulting ADP (pink) and phosphate are released. SpoIVA at high concentrations forms filaments (upper arrow). At low concentrations, SpoIVA undergoes a conformational change (obtuse triangle) that is polymerization-competent once the protein concentration is raised above the threshold. Below, a sporulating cell is shown in which we hypothesize that the SpoIVA concentration in the mother cell is below the threshold. Recruitment of SpoIVA to the forespore surface (*Right*) could increase the local concentration of SpoIVA above the threshold, which may drive polymerization of SpoIVA at the correct place and time. Fig. S7 is identical to Fig. P1 in the *Author Summary*.

Table S1. *Bacillus subtilis* strains used in this study

Strain	Genotype	Source
PY79	Prototrophic derivative of *B. subtilis* 168	(1)
KP73	Δ*spoIVA::neo*	(2)
KR394	Δ*spoIVA::neo thrC::spoIVA wt spec*	(3)
JPC75	Δ*spoIVA::neo thrC::spoIVA D97A spec*	This study
JPC269	Δ*spoIVA::neo thrC::spoIVA T70A spec*	This study
JPC278	Δ*spoIVA::neo thrC:: spoIVA T71A spec*	This study
JPC221	Δ*spoIVA::neo thrC::spoIVA T70A-T71A spec*	This study
KR217	*thrC::spoIVA wt spec*	(3)
JPC74	*thrC::spoIVA D97A spec*	This study
JPC219	*thrC::spoIVA T70A-T71A spec*	This study
JPC156	Δ*spoIVA::neo amyE::spoIVA wt cat thrC::GFP-spoIVA wt spec*	This study
JPC174	Δ*spoIVA::neo amyE::spoIVA D97A cat thrC::GFP-spoIVA D97A spec*	This study
JPC243	Δ*spoIVA::neo amyE::spoIVA T70A-T71A cat thrC::GFP-spoIVA T70A-T71A spec*	This study
KR448	Δ*spoIVA::neo cotE::pCW13 (cotE-gfp) cat thrC::spoIVA wt spec*	(3)
JPC138	Δ*spoIVA::neo cotE::pCW13 (cotE-gfp) cat thrC::spoIVA D97A spec*	This study
JPC281	Δ*spoIVA::neo cotE::pCW13 (cotE-gfp) cat thrC::spoIVA T70A-T71A spec*	This study

1. Youngman P, Perkins JB, Losick R (1984) Construction of a cloning site near one end of Tn917 into which foreign DNA may be inserted without affecting transposition in *Bacillus subtilis* or expression of the transposon-borne erm gene. *Plasmid* 12(1):1–9.
2. Price KD, Losick R (1999) A four-dimensional view of assembly of a morphogenetic protein during sporulation in *Bacillus subtilis*. *J Bacteriol* 181(3):781–790.
3. Ramamurthi KS, Losick R (2008) ATP-driven self-assembly of a morphogenetic protein in *Bacillus subtilis*. *Mol Cell* 31(3):406–414.

Table S2. Sporulation efficiencies of strains harboring various *IVA* alleles

Strain*	*IVA*	*thrC*	Sporulation efficiency†
A	WT	—	1
B	Δ	—	$<10^{-8}$
C	Δ	IVA^{WT}	1.5
D	Δ	IVA^{D97A}	$2{\cdot}10^{-7}$
E	Δ	$IVA^{T70A\text{-}T71A}$	$0.9{\cdot}10^{-5}$
F	Δ	IVA^{T70A}	$5.6{\cdot}10^{-3}$
G	Δ	IVA^{T71A}	1
H	WT	IVA^{WT}	1.2
I	WT	IVA^{D97A}	0.7
J	WT	$IVA^{T70A\text{-}T71A}$	1.4

*Strain A: PY79, strain B: KP73, strain C: KR394, strain D: JPC75, strain E: JPC221, strain F: JPC269, strain G: JPC278, strain H: KR217, strain I: JPC74, strain J: JPC219. Genotypes are listed in Table S1.

†Spores per milliliter recovered, relative to PY79 (WT). PY79 routinely yielded about 1.5×10^8 spores per milliliter.